Variational superposed Gaussian approximation for time-dependent solutions of Langevin equations

Yoshihiko Hasegawa*

Department of Information and Communication Engineering, Graduate School of Information Science and Technology, The University of Tokyo, Tokyo 113-8656, Japan

(Received 21 November 2014; published 21 April 2015)

We propose a variational superposed Gaussian approximation (VSGA) for dynamical solutions of Langevin equations subject to applied signals, determining time-dependent parameters of superposed Gaussian distributions by the variational principle. We apply the proposed VSGA to systems driven by a chaotic signal, where the conventional Fourier method cannot be adopted, and calculate the time evolution of probability density functions (PDFs) and moments. Both white and colored Gaussian noises terms are included to describe fluctuations. Our calculations show that time-dependent PDFs obtained by VSGA agree excellently with those obtained by Monte Carlo simulations. The correlation between the chaotic input signal and the mean response are also calculated as a function of the noise intensity, which confirms the occurrence of aperiodic stochastic resonance with both white and colored noises.

DOI: 10.1103/PhysRevE.91.042912 PACS number(s): 05.45.−a, 02.60.−x, 05.10.Gg

I. INTRODUCTION

Langevin equations can model systems subject to fluctuations and hence have many applications in diverse research fields such as physics, chemistry, financial engineering, and biology [1–3]. Without a driving force, systems subject to white Gaussian noise relax to their stationary states. For one-dimensional stationary systems, the probability density function (PDF) can be obtained in a closed form for many cases. However, in the presence of a driving force, its time-dependent solution is rarely available even for one-dimensional systems. Recent advancements in nonequilibrium theory [4,5] strongly demand reliable methods for time-dependent solutions of Langevin equations for systems driven by time-dependent external forces. The moment method (MM) is widely used to study dynamics [6–8]; it considers the time evolution of moments of PDFs [in most cases, up to the second-order moments (mean and variance) are considered]. If we truncate at the second moment (i.e., nth-order terms where $n \geqslant 3$ are ignored), the number of differential equations is $N(N+3)/2$, where N is the dimensionality of the model; thus, with current computer capabilities, the MM is tractable up to relatively large N. Although the MM can provide satisfactory results for linear (or weakly nonlinear) systems, its applicability collapses even for simple bistable models. Here, for time-dependent solutions of Langevin equations, we propose an approximation technique in which PDFs are represented by superposed multiple Gaussian distributions, obtaining time-evolution equations for parameters of each of the Gaussian distributions with the variational principle. We call the proposed method the variational superposed Gaussian approximation (VSGA). Dynamical Gaussian approximations have a long history in quantum mechanics. Heller introduced the Gaussian wave-packet method [9], which approximates time-dependent solutions of Schrödinger equations with a Gaussian packet by obtaining equations for the mean and variance through the McLachlan variational principle [10] (other equivalent variational principles are also known [11–13] and this is a special case of the weighted residual method). Several researchers extended Heller's approach to incorporate multiple Gaussian distributions [14–16], and these methods can provide reliable solutions for time-dependent wave functions by virtue of their multiplicity. Although the effectiveness of the multiple Gaussian method with the variational principle has been shown to approximate time-dependent wave functions [14–16], its capability has not been shown in the context of time-dependent Fokker-Planck equations (FPEs).

After the Gaussian wave-packet approximations in quantum mechanics, several studies employed a superposition of Gaussian distributions for Langevin equations [17–19]. Reference [17] adopted superposed Gaussian distributions to approximate stationary solutions through the weighted residual method. For dynamical solutions, Ref. [18] employed superposed Gaussian distributions based on the statistical equivalent linearization where PDFs are represented by small elements of Gaussian distributions. It was noted that Pradlwarter's method has to manage the variance and the number of Gaussian distributions during the propagation. Similarly, Terejanu *et al.* [19] developed an approximation scheme based on superposed Gaussian distributions, which calculated the mean and variance with a fixed weight. After calculating the mean and variance, they optimized the weight, using quadratic programming to minimize the squared error. Unlike these approaches, the VSGA does not require such extra steps; it directly calculates the mean, variance, and weight in a unified way. Reference [20] approximates time-dependent solutions with exponential of a polynomial function to obtain the time-evolution equations of parameters through the weighted residual method. However, such an approximation has difficulty in satisfying the normalization condition during the time evolution. There are several numerical approaches to the study of the dynamics of FPEs that represent PDFs by using complete set functions (e.g., a matrix continued-fraction method; for details, see Ref. [21] and the references therein). More-direct numerical schemes, such as a finite-element method [22,23] and a finite-difference method [24], have also been studied. These approaches, however, have high computational costs and hence are not suited for time-dependent solutions.

*Corresponding author: yoshihiko.hasegawa@gmail.com

To investigate the effectiveness of VSGA, we applied it to a quartic bistable system subject to white or colored noise. Although a bistable system can describe switching dynamics and has many and varied applications to realistic problems [25], its nonlinearity makes the application of the simple MM difficult. We consider a system driven by a chaotic signal (the Rössler oscillator). When the signal is aperiodic, we cannot use a Fourier series expansion, as is often employed for periodic cases [26], and hence many studies have resorted to using direct Monte Carlo (MC) simulations. We show that VSGA can accurately approximate the time-dependent moments and the PDFs of the systems for both white (one-dimensional) and colored (two-dimensional) noises. Calculating the correlation between the chaotic input signal and the mean of the dynamics [cf. Eq. (27)], we show that the correlation is maximal when the noise is of intermediate strength; this is a signature of aperiodic stochastic resonance (ASR) [27,28] [for general stochastic resonance (SR), see [29–33] and the references therein]. Furthermore, from the results with colored noise, we show that the time correlation weakens the magnitude of the ASR.

The remainder of this paper is organized as follows. In Sec. II, we introduce our proposed method, the VSGA, and provide a detailed explanation of the variational principle for FPEs. We obtain implicit differential equations that should be satisfied by the mean, variance, and weights of each of the Gaussian distributions. In Sec. III, we investigate the effectiveness of VSGA by applying it to two cases: a bistable system driven by a chaotic signal subject to white noise (Sec. III A) and colored noise (Sec. III B). Finally, we provide a discussion and present our conclusions in Sec. IV.

II. METHODS

We consider an N-dimensional Langevin equation (the Stratonovich interpretation),

$$\frac{dx_i}{dt} = f_i(\boldsymbol{x},t) + \sum_{j=1}^{N_g} g_{ij}(\boldsymbol{x},t)\xi_j(t), \quad (i = 1,2,\ldots,N), \quad (1)$$

where $\boldsymbol{x} = (x_1,\ldots,x_N)^\top$ ($\top$ denotes the transpose operation) is an N-dimensional column vector, $f_i(\boldsymbol{x},t)$ and $g_{ij}(\boldsymbol{x},t)$ denote drift and multiplicative terms, respectively, $\xi_i(t)$ is white Gaussian noise with the correlation $\langle \xi_i(t)\xi_j(t')\rangle = 2\delta_{ij}\delta(t-t')$, and N_g is the number of noise sources [21]. The Langevin equation (1) has the corresponding FPE [21],

$$\frac{\partial}{\partial t}P(\boldsymbol{x};t) = \hat{L}(\boldsymbol{x},t)P(\boldsymbol{x};t), \quad (2)$$

where $P(\boldsymbol{x};t)$ is the probability density of $\boldsymbol{x}$ at time t, and $\hat{L}(\boldsymbol{x},t)$ is an FPE operator defined by

$$\hat{L}(\boldsymbol{x},t) = -\sum_i \frac{\partial}{\partial x_i}F_i(\boldsymbol{x},t) + \sum_{i,j}\frac{\partial^2}{\partial x_i \partial x_j}G_{ij}(\boldsymbol{x},t). \quad (3)$$

Here $F_i(\boldsymbol{x},t) = f_i(\boldsymbol{x},t) + \sum_{k,j} g_{kj}(\boldsymbol{x},t)\partial_{x_k} g_{ij}(\boldsymbol{x},t)$ and $G_{ij}(\boldsymbol{x},t) = \sum_k g_{ik}(\boldsymbol{x},t)g_{jk}(\boldsymbol{x},t)$ [note that the VSGA can be applied to the Itô interpretation by modifying $F_i(\boldsymbol{x},t)$] [21]. We are interested in a time-dependent solution $P(\boldsymbol{x};t)$ of Eq. (2). We approximate the time evolution by using the variational principle, which is explained below for the FPE.

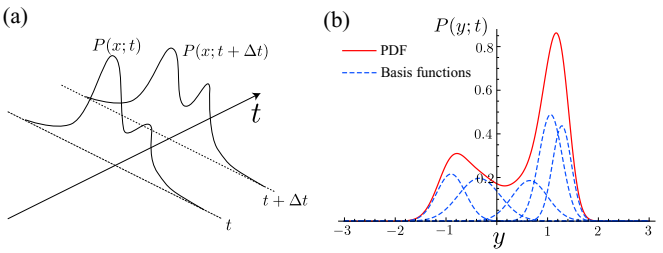

FIG. 1. (Color online) (a) Illustration of time evolution of a PDF. If the PDF at time t [i.e., $P(x;t)$] is known, the optimal $P(x;t+\Delta t)$ is given by $P(x;t+\Delta) \simeq P(x;t) + \Delta t\Theta(x;t)$, where $\Theta(x;t)$ is optimal. (b) Example of an approximative PDF (solid line) that is a superposition of five Gaussian distributions (dashed lines).

Let $\Theta(\boldsymbol{x};t)$ be the time derivative of $P(\boldsymbol{x};t)$, i.e., $\Theta(\boldsymbol{x};t) = \dot{P}(\boldsymbol{x};t)$. We focus on a specific time t, where $P(\boldsymbol{x};t)$ is already known, and we want to know the optimal time evolution $\Theta(\boldsymbol{x};t)$ [Fig. 1(a)]. In other words, we want to calculate $P(\boldsymbol{x};t+\Delta t)$, where Δt is a sufficiently small increment, from a known $P(\boldsymbol{x};t)$ by using $P(\boldsymbol{x};t+\Delta t) \simeq P(\boldsymbol{x};t) + \Delta t\Theta(\boldsymbol{x};t)$. From Eq. (2), the optimal $\Theta(\boldsymbol{x};t)$ should minimize

$$R[\Theta] = \int_{-\infty}^{\infty}\{\hat{L}(\boldsymbol{x},t)P(\boldsymbol{x};t) - \Theta(\boldsymbol{x};t)\}^2 d\boldsymbol{x}, \quad (4)$$

where we have abbreviated as follows: $\int_{-\infty}^{\infty} dx_1 \cdots \int_{-\infty}^{\infty} dx_N = \int_{-\infty}^{\infty} d\boldsymbol{x}$. Although we may obtain the optimal $P(\boldsymbol{x};t+\Delta t)$ by solving Eq. (4) with respect to Θ, the optimal Θ does not necessarily yield solutions that satisfy the normalization condition $\int_{-\infty}^{\infty} P(\boldsymbol{x};t)d\boldsymbol{x} = 1$ at any time t. Therefore, we should impose an additional constraint on Eq. (4). When $P(\boldsymbol{x};t)$ is normalized at $t = 0$, then the normalization of $P(\boldsymbol{x};t)$ at $t > 0$ is satisfied by the equation given by

$$\frac{d}{dt}\int_{-\infty}^{\infty} P(\boldsymbol{x};t)d\boldsymbol{x} = \int_{-\infty}^{\infty}\Theta(\boldsymbol{x};t)d\boldsymbol{x} = 0. \quad (5)$$

Therefore, to minimize Eq. (4) with the normalization condition of Eq. (5), we consider the equation

$$\tilde{R}[\Theta] = \int_{-\infty}^{\infty}\{\hat{L}(\boldsymbol{x},t)P(\boldsymbol{x};t) - \Theta(\boldsymbol{x};t)\}^2 d\boldsymbol{x} + \lambda(t)\int_{-\infty}^{\infty}\Theta(\boldsymbol{x};t)d\boldsymbol{x}, \quad (6)$$

where λ is the Lagrange multiplier. With a variation of $\delta\Theta(\boldsymbol{x};t)$ in Eq. (6), $\delta\tilde{R}$ should vanish for the optimal $\Theta(\boldsymbol{x};t)$, yielding

$$\int_{-\infty}^{\infty}\delta\Theta\{\hat{L}(\boldsymbol{x},t)P(\boldsymbol{x};t) - \Theta(\boldsymbol{x};t) + \lambda(t)\}d\boldsymbol{x} = 0, \quad (7)$$

where we redefined λ for notational convenience. Suppose $P(\boldsymbol{x};t)$ is a function parametrized by time-dependent K values $\boldsymbol{\theta}(t) = (\theta_1(t),\theta_2(t),\ldots,\theta_K(t))$,

$$P(\boldsymbol{x};t) = P(\boldsymbol{x};\boldsymbol{\theta}(t)), \quad (8)$$

where the time-dependence of $P(\boldsymbol{x};t)$ is represented through $\boldsymbol{\theta}(t)$. Thus, $\Theta(\boldsymbol{x};t)$ is given by

$$\Theta(\boldsymbol{x};t) = \Theta(\boldsymbol{x};\boldsymbol{\theta}(t),\dot{\boldsymbol{\theta}}(t)). \tag{9}$$

The variation $\delta\Theta$ can be achieved only through the variation $\delta\dot{\boldsymbol{\theta}}$ [$\boldsymbol{\theta}$ cannot be changed, as we assumed that $P(\boldsymbol{x};t) = P(\boldsymbol{x};\boldsymbol{\theta}(t))$ is fixed at time t]:

$$\delta\Theta = \sum_{\ell=1}^{K} \frac{\partial\Theta(\boldsymbol{x};\boldsymbol{\theta},\dot{\boldsymbol{\theta}})}{\partial\dot{\theta}_\ell}\delta\dot{\theta}_\ell, \tag{10}$$

where

$$\frac{\partial\Theta(\boldsymbol{x};\boldsymbol{\theta},\dot{\boldsymbol{\theta}})}{\partial\dot{\theta}_\ell} = \frac{\partial}{\partial\dot{\theta}_\ell}\frac{dP(\boldsymbol{x};\boldsymbol{\theta})}{dt} = \frac{\partial}{\partial\dot{\theta}_\ell}\left[\sum_{\ell'=1}^{K}\frac{\partial P(\boldsymbol{x};\boldsymbol{\theta})}{\partial\theta_{\ell'}}\dot{\theta}_{\ell'}\right] = \frac{\partial P(\boldsymbol{x};\boldsymbol{\theta})}{\partial\theta_\ell}. \tag{11}$$

For the variation $\delta\dot{\boldsymbol{\theta}} = (\delta\dot{\theta}_1,\ldots,\delta\dot{\theta}_K)$, we consider the simplest orthogonal case:

$$\delta\dot{\boldsymbol{\theta}} = (1,0,0,\ldots,0),(0,1,0,\ldots,0),\ldots,(0,0,0,\ldots,1).$$

Substituting Eqs. (10) and (11) into Eq. (7), we have K constraints

$$\int_{-\infty}^{\infty}\frac{\partial P(\boldsymbol{x};\boldsymbol{\theta})}{\partial\theta_\ell}\{\hat{L}(\boldsymbol{x},t)P(\boldsymbol{x};\boldsymbol{\theta}) - \Theta(\boldsymbol{x};\boldsymbol{\theta},\dot{\boldsymbol{\theta}}) + \lambda(t)\}d\boldsymbol{x} = 0 \quad (\ell = 1,2,\ldots,K), \tag{12}$$

which is the variational principle for FPEs that is equivalent to the McLachlan one. Also, Eq. (12) without λ can be seen as minimizing the residual with a weight function $\partial_{\theta_\ell}P(\boldsymbol{x};\boldsymbol{\theta})$.

We next show an explicit form of $P(\boldsymbol{x};\boldsymbol{\theta}(t))$. We approximate $P(\boldsymbol{x};t)$ with a superposition of multiple Gaussian distributions [Fig. 1(b)],

$$P(\boldsymbol{x};\boldsymbol{\theta}(t)) = \sum_{m=1}^{N_B} r_m g(\boldsymbol{x};\boldsymbol{A}_m(t),\boldsymbol{b}_m(t)), \tag{13}$$

where $g(\boldsymbol{x};\boldsymbol{A},\boldsymbol{b})$ is an un-normalized Gaussian distribution:

$$g(\boldsymbol{x};\boldsymbol{A},\boldsymbol{b}) = \exp(-\boldsymbol{x}^\top\boldsymbol{A}\boldsymbol{x} + \boldsymbol{b}^\top\boldsymbol{x}). \tag{14}$$

Here $\boldsymbol{A}$ is an $N\times N$ symmetric matrix (positive definite), $\boldsymbol{b}$ is an N-dimensional column vector, r_m is a parameter that combines the weight of the mth Gaussian with a normalization constant, and N_B is the number of basis functions. We employed a parametrization of Eq. (14) that is different from the conventional multivariate Gaussian representation, because multidimensional calculations are easier with Eq. (14) (cf. Appendix A). For instance, multiplication is simply given by

$$g(\boldsymbol{x};\boldsymbol{A}_m,\boldsymbol{b}_m)g(\boldsymbol{x};\boldsymbol{A}_{m'},\boldsymbol{b}_{m'}) = g(\boldsymbol{x};\boldsymbol{A}_m+\boldsymbol{A}_{m'},\boldsymbol{b}_m+\boldsymbol{b}_{m'}).$$

We optimized all of the Gaussian parameters by using the variational principle, i.e., $\boldsymbol{\theta} = (\boldsymbol{A}_m,\boldsymbol{b}_m,r_m)_{m=1}^{N_B}$. For an N-dimensional system and N_B basis functions, the total number of parameters is

$$K = \frac{N_B(N+1)(N+2)}{2}. \tag{15}$$

From Eq. (12) and the constraint of Eq. (5), we obtain $(K+1)$ implicit differential equations of the following form:

$$H_\ell(\boldsymbol{\theta}(t),\dot{\boldsymbol{\theta}}(t),\lambda(t),t) = 0, \quad \ell = 1,2,\ldots,K,K+1. \tag{16}$$

Equation (16) is called a differential algebraic equation (DAE) [34]. Because the dimensionality of $(\dot{\boldsymbol{\theta}}(t),\lambda(t))$ is $K+1$ and there are $K+1$ equations, we can uniquely specify $(\dot{\boldsymbol{\theta}}(t),\lambda(t))$ given $\boldsymbol{\theta}(t)$. However, because it is very difficult to explicitly solve Eq. (16) with respect to $(\dot{\boldsymbol{\theta}}(t),\lambda(t))$ for higher dimensional cases, we use a DAE solver in *Mathematica 10* (NDSolve function). VSGA does not accept arbitrary initial values, because $(\boldsymbol{A}_m,\boldsymbol{b}_m,r_m)_{m=1}^{N_B}$ should satisfy the normalizing condition, which can be obtained from Eqs. (A3)–(A5) (cf. Appendix B).

III. RESULTS

We applied the VSGA to two double-well systems driven by chaotic signals, one subject to white Gaussian noise (Sec. III A) and the other subject to colored Gaussian noise (Sec. III B). We also performed MC simulations to show the reliability of the VSGA.

A. Chaotically driven bistable potential subject to white noise

We applied the VSGA to a driven bistable potential subject to white Gaussian noise. Specifically, we applied it to a one-dimensional potential driven by an input signal $I(t)$,

$$\frac{dy}{dt} = y - y^3 + I(t) + \sqrt{D}\xi(t), \tag{17}$$

where D is the noise intensity and $\xi(t)$ is white Gaussian noise with the correlation $\langle\xi(t)\xi(t')\rangle = 2\delta(t-t')$. The FPE operator $\hat{L}(\boldsymbol{x},t) = \hat{L}(y,t)$ is given by

$$\hat{L}(y,t) = -\frac{\partial}{\partial y}\{y - y^3 + I(t)\} + D\frac{\partial^2}{\partial y^2}. \tag{18}$$

Substituting Eq. (18) into Eq. (12), we can calculate K coupled DAEs with respect to $\boldsymbol{\theta} = (\boldsymbol{A}_m,\boldsymbol{b}_m,r_m)_{m=1}^{N_B}$ (for the one-dimensional case, $\boldsymbol{A}_m = a_m$ and $\boldsymbol{b}_m = b_m$, where a_m,b_m are real scalar quantities), requiring moments of the Gaussian distribution of up to the sixth order [$\int_{-\infty}^{\infty} y^{n_y}g(y;\boldsymbol{A},\boldsymbol{b})dy$, with $n_y \leqslant 6$]. For the one-dimensional case, the normalization constraint is

$$\frac{d}{dt}\int_{-\infty}^{\infty}P(\boldsymbol{x};\boldsymbol{\theta}(t))d\boldsymbol{x} = \frac{d}{dt}\int_{-\infty}^{\infty}\sum_{m=1}^{N_B}r_m(t)\exp[-a_m(t)y^2 + b_m(t)y]dy = 0, \tag{19}$$

yielding

$$0 = \sum_{m=1}^{N_B}\frac{\sqrt{\pi}}{4a_m(t)^{5/2}}[4a_m(t)^2\dot{r}_m(t) - 2a_m(t)r_m(t) \times \{\dot{a}_m(t) - b_m(t)\dot{b}_m(t)\} - b_m(t)^2\dot{a}_m(t)r_m(t)]\exp\left[\frac{b_m(t)^2}{4a_m(t)}\right]. \tag{20}$$

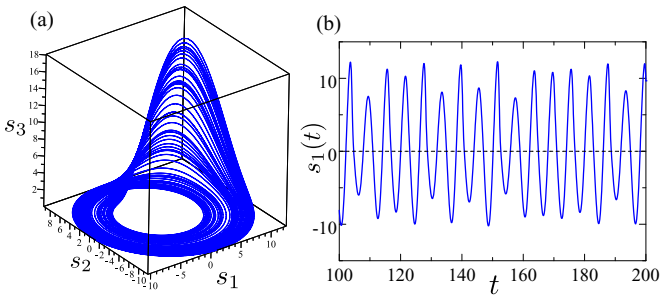

FIG. 2. (Color online) Trajectories of Rössler chaos [Eqs. (21)–(23)]: (a) 3D plot of s_1, s_2, and s_3; and (b) s_1 as a function of t. The parameters are $c_1 = 0.15$, $c_2 = 0.2$, and $c_3 = 7.1$.

Equation (20) should be solved along with the DAEs obtained from Eq. (12); the total dimensionality of the DAEs is $K + 1$.

For the input signal $I(t)$, we used the Rössler oscillator [35]:

$$\frac{ds_1}{dt} = -s_2 - s_3, \tag{21}$$

$$\frac{ds_2}{dt} = s_1 + c_1 s_2, \tag{22}$$

$$\frac{ds_3}{dt} = c_2 + s_3(s_1 - c_3). \tag{23}$$

Here c_i are parameters of the oscillator, and we used $c_1 = 0.15$, $c_2 = 0.2$, and $c_3 = 7.1$ (identical to the values used in Ref. [36]), with which Eqs. (21)–(23) exhibit chaotic dynamics. Figures 2(a) and 2(b) show trajectories of the Rössler oscillator for (a) s_1, s_2, and s_3 and (b) s_1 as a function of time t. The average peak-to-peak interval (which corresponds to the period of the oscillations) of $s_1(t)$ is about 6. We define the input signal as

$$I(t) = \alpha s_1(\omega t), \tag{24}$$

where α is the input strength and ω is the reciprocal of the time scale (this corresponds to the angular frequency of the periodic oscillations). Although time-dependent solutions of periodically driven systems are often represented as a Fourier series expansion [26], such an expansion cannot be used for a chaotically driven system.

We first study a stationary case [i.e., $I(t) = \kappa$, where κ is a constant parameter], because stationary PDFs can be obtained analytically for a quartic potential. Note that the VSGA in a stationary case is essentially equivalent to that given in Ref. [17]. The stationary PDF $P_{st}(y)$ is given by

$$P_{st}(y) = \frac{1}{Z(D)} \exp\left[-\frac{U(y)}{D}\right], \tag{25}$$

where $Z(D) = \int_{-\infty}^{\infty} \exp[-U(y)/D]dy$ (numerically integrated) and $U(x)$ is a potential function $U(y) = -\int(y - y^3 + \kappa)dy = y^4/4 - y^2/2 - \kappa y$. The stationary PDF of a VSGA is obtained by letting the system evolve for a long enough time when it equilibrates. Although in the VSGA calculations with larger N_B can yield more accurate results, we employed $N_B = 5$ (total parameter size is $K = 15$ [Eq. (15)]) because numerical instability occurs for excessively large N_B due to the nonorthogonality of multiple Gaussian distributions. Figure 3 shows the stationary distributions of the VSGA ($N_B = 5$; dashed line) and the analytic solutions obtained for Eq. (25) (solid line) for (a) $D = 0.2$ and $\kappa = 0$, (b) $D = 1.0$ and $\kappa = 0$, and (c) $D = 0.5$ and $\kappa = 0.1$. In all parameter settings, the VSGA shows very good agreement with the analytical solutions, including the asymmetric case [Fig. 3(c)]. In Figs. 3(a)–3(c), the dot-dashed lines denote the Gaussian bases constituting the PDFs of the VSGA; we can see that two bases each are located near the deterministic stable steady states ($y = \pm 1$) and one near the deterministic unstable steady state ($y = 0$). In Figs. 3(a)–3(c), the insets describe tails of PDFs with lot plots, where we see that tails of VSGA decay slightly slower than analytical solutions; this is because tails of VSGA are $\exp[-O(y^2)]$ (Gaussian), while the analytical ones are $\exp[-O(y^4)]$. There is a small deviation in VSGA solutions around $y = 0$ and it is considered that the deviation compensates slow decay at tails of the PDFs. We next see a relation between N_B and an error ϵ of the approximation by calculating distance between analytic and VSGA stationary PDFs:

$$\epsilon = \int_{-\infty}^{\infty} \{P_{st}(y) - P(y;\boldsymbol{\theta})\}^2 dy. \tag{26}$$

Figure 4 shows the error ϵ as a function of N_B with a log plot, where circles and a line denote ϵ and its fitting line

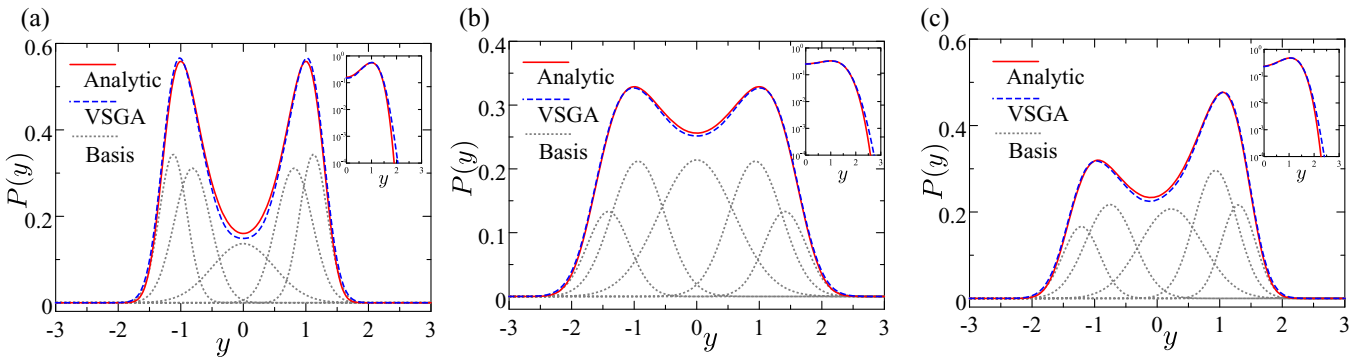

FIG. 3. (Color online) Stationary PDFs obtained by analytic calculation of Eq. (25) (solid line) and by the VSGA with $N_B = 5$ (dashed line) for (a) $D = 0.2$ and $\kappa = 0$, (b) $D = 1.0$ and $\kappa = 0$, and (c) $D = 0.5$ and $\kappa = 0.1$. In (a)–(c), the dotted lines denote each of the single bases of the VSGA. The insets show log plots of PDFs at tail regions.

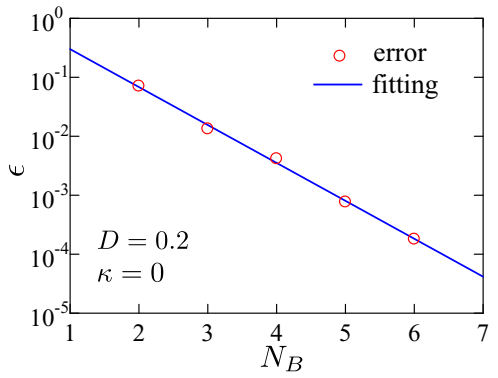

FIG. 4. (Color online) Error ϵ [Eq. (26)] of VSGA as a function of N_B for the one-dimensional stationary case, where circles and a line denote ϵ and its fitting curve, respectively (the curve is $\ln\epsilon = -1.48N_B + 0.28$). Parameters are $D = 0.2$ and $\kappa = 0$.

($\ln\epsilon = -1.48N_B + 0.28$), respectively. We see that the error ϵ decreases exponentially as a function of N_B.

We next studied the dynamical case where the input $I(t)$ is given by Eq. (24). Figure 5 displays the $P(y;t)$ as functions of y and t, which are calculated by the VSGA with $N_B = 5$, for (a) $D = 0.2$, $\alpha = 0.02$, and $\omega = 0.5$; (b) $D = 1.0$, $\alpha = 0.02$, and $\omega = 0.5$; and (c) $D = 0.2$, $\alpha = 0.02$, and $\omega = 0.25$. To verify the $P(y;t)$ calculated by the VSGA, we evaluated the accuracy of the PDFs $P(y;t)$ at time $t = 100$ by calculating the VSGA and by performing MC simulations (we selected $t = 100$ so that we could ignore the effects of the initial values). For the MC simulations, the PDFs were constructed by repeating the stochastic simulations 100 000 times (time resolution is 0.0001). Figures 6(a)–6(c) show the PDFs calculated by the MC simulations (circles), the VSGA (dashed line), and each of the bases of the VSGA (dotted line). The parameter settings for panels (a), (b), and (c) correspond to those in Figs. 5(a)–5(c), respectively. For all parameter settings, the PDFs of the VSGA are in excellent agreement with those obtained by the MC simulations; this verifies the reliability of the VSGA with respect to the PDFs at a specified time.

In order to see the dynamical aspects of the VSGA, we also compared the mean $\langle y(t)\rangle$ obtained by the MC simulations to that obtained by the VSGA for the interval $t = 100$–200 (we did not consider the interval $t = 0$–100 because of the initial value effects). In Figs. 7(a)–7(c), we show the mean $\langle y(t)\rangle$ calculated by the MC simulations (dashed line), the VSGA with $N_B = 5$ (solid line), and the VSGA with $N_B = 1$ (dot-dashed line). The parameter settings for (a), (b), and (c) correspond to those used in Figs. 5(a)–5(c), respectively. For the MC simulations, we repeated the Langevin equations with the same chaotic signal 10 000 times to calculate the average. Along with results of VSGA with $N_B = 5$ plotted by solid lines, dot-dashed lines show those calculated by the VSGA with $N_B = 1$, which is similar to the MM case. In Figs. 7(a)–7(c), we can see that the mean $\langle y(t)\rangle$ of the values obtained by the VSGA with $N_B = 5$ are in excellent agreement with that of the MC simulations, but not with that of the $N_B = 1$ model. The mean of the $N_B = 1$ values is located near 1 and it only approximates one of the two wells (the mean would be distributed around -1 for particular different initial values).

In order to study the properties of the VSGA in more detail, we considered the time evolution of the parameters of each of the Gaussian bases for $N_B = 5$. Figures 8(a)–8(c) show the mean μ_m, standard deviation σ_m, and weight q_m, respectively, of each Gaussian basis as a function of time t [μ_m, σ_m, and q_m were calculated by a_m, b_m, and r_m with Eqs. (A6)–(A8)]; the parameters were $D = 0.2, \alpha = 0.02$, and $\omega = 0.25$ identical to those used in Fig. 5(c). In Figs. 8(a)–8(c), solid, dashed, dotted, dot-dashed, and long-dashed lines represent the quantities of the 1st, 2nd, . . . , 5th Gaussian bases, respectively. In Fig. 8(a), which shows the time evolution of the mean μ_m, we can see that the two wells are each approximated by two Gaussian distributions, and the temporal variation of the mean is at most $\sim$1 (cf. 5th basis; long-dashed line). From the time evolution of the standard deviation σ_m [Fig. 8(b)], we see that the temporal variation as a function of time is small (about $\sim$0.1), although the standard deviation averaged over time is different for each basis. In Fig. 8(c), all the weights q_m are distributed around 0.2, which shows that all of the bases contributed to the PDF. Because the VSGA approximates the two wells with more than two Gaussian distributions, the mean properly approximates the exact time evolution.

Driven bistable systems subject to noise are often characterized by the maximal signal-to-noise ratio under adequate noise strength (SR). Although SR was originally studied in periodic signals, Refs. [27,28] studied the SR effects in aperiodic signals. We quantified the extent of SR for aperiodic signals as

$$C_0 = \overline{I(t)\langle y(t+\mathscr{T}_0)\rangle}, \tag{27}$$

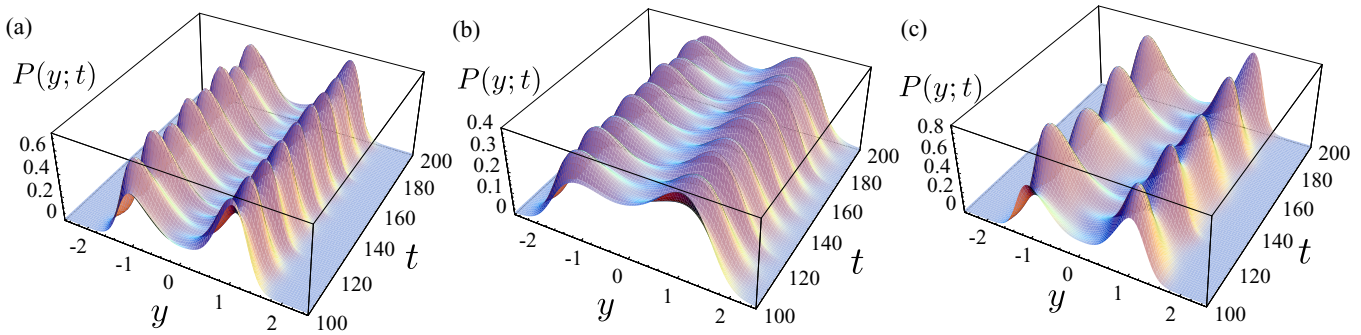

FIG. 5. (Color online) Dynamical PDFs $P(y;t)$ as functions of y and t obtained by the VSGA with $N_B = 5$ for (a) $D = 0.2$, $\alpha = 0.02$, and $\omega = 0.5$; (b) $D = 1.0$, $\alpha = 0.02$, and $\omega = 0.5$; and (c) $D = 0.2$, $\alpha = 0.02$, and $\omega = 0.25$.

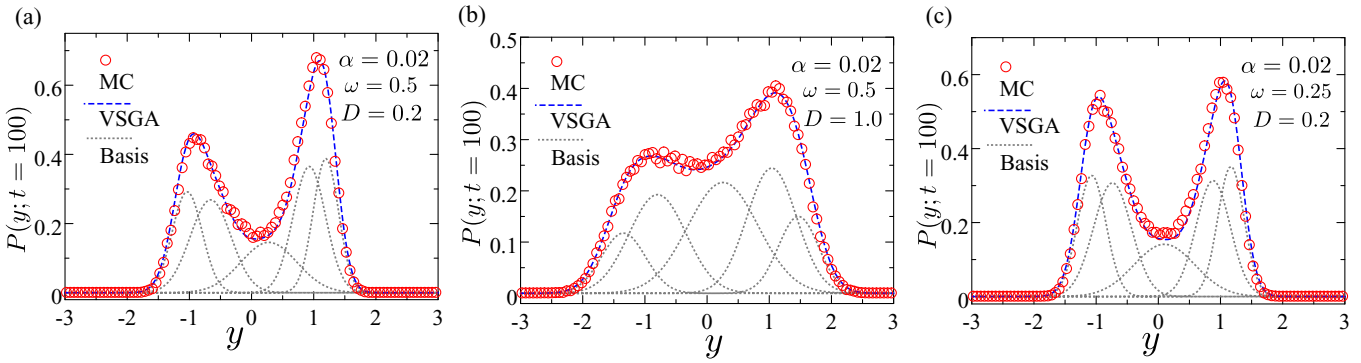

FIG. 6. (Color online) PDFs $P(y;t)$ at time $t = 100$ obtained by MC simulations (circles), the VSGA with $N_B = 5$ (dashed line), and each of the Gaussian bases of the VSGA (dotted line). The parameters in panels (a)–(c) are the same as in Figs. 5(a)–5(c), respectively.

with

$$\overline{\mathcal{F}(t)} = \frac{1}{T}\int_{t_0}^{t_0+T} \mathcal{F}(t)dt,$$

where $\mathcal{F}(t)$ is an arbitrary time-dependent function, t_0 is the starting time, and T is the duration of the observation; we again set $t_0 = 100$ and $T = 200$. In Eq. (27), $\mathscr{T}_0$ is time lag yielding the maximal correlation

$$\mathscr{T}_0 = \underset{\mathscr{T}}{\text{argmax}}\, \overline{I(t)\langle y(t+\mathscr{T})\rangle}. \tag{28}$$

Here C_0 evaluates the amount of chaotic information transmitted, and a larger value corresponds to better transmission. Although the SR for a chaotic signal was studied in view of noise-induced phase synchronization [36], the ASR obtained by calculating the correlation of Eq. (27) has not yet been studied. Figure 9 shows (a) the correlation C_0 and (b) the time lag $\mathscr{T}_0$ as a function the noise intensity D, where C_0 for the VSGA with $N_B = 5$ is shown by a solid line and that for the MC simulations is shown by circles. Note that VSGA could not calculate solutions for $D < 0.15$ (see the discussion). The parameters were $\alpha = 0.02$ and $\omega = 0.5$. C_0 achieves a maximum at $D \simeq 0.35$, which indicates the occurrence of ASR. Comparing the VSGA and MC results shown in Figs. 9(a) and 9(b), we see very good agreement, which verifies the reliability the VSGA. By using the VSGA, we can calculate properties of chaotically driven systems without performing stochastic simulations.

B. Chaotically driven bistable potential with colored noise

We next apply the VSGA to a bistable system with colored Gaussian noise. The one-dimensional colored Gaussian noise system can be embedded into a two-dimensional Langevin equation with white Gaussian noise,

$$\frac{dy}{dt} = y - y^3 + I(t) + z(t), \tag{29}$$

$$\frac{dz}{dt} = -\frac{z}{\tau} + \frac{\sqrt{D}}{\tau}\xi(t), \tag{30}$$

where $\xi(t)$ is white Gaussian noise $[\langle \xi(t)\xi(t')\rangle = 2\delta(t-t')]$, $I(t)$ is the input signal, τ is the correlation time, and $z(t)$ (the Ornstein-Uhlenbeck process) corresponds to a colored noise with the correlation $\langle z(t)z(t')\rangle = (D/\tau)\exp(-|t-t'|/\tau)$. We also employed the Rössler input for $I(t)$ [Eq. (24)]. The FPE operator $\hat{L}(y,z,t)$ of Eqs. (29) and (30) is

$$\hat{L}(y,z,t) = -\frac{\partial}{\partial y}[y - y^3 + z + I(t)] + \frac{1}{\tau}\frac{\partial}{\partial z}z + \frac{D}{\tau^2}\frac{\partial^2}{\partial z^2}. \tag{31}$$

Substituting Eq. (31) into Eq. (12), we can again calculate the K (the number of total parameters) coupled DAE with respect to $\boldsymbol{\theta} = (\boldsymbol{A}_m, \boldsymbol{b}_m, r_m)_{m=1}^{N_B}$, with

$$\boldsymbol{A}_m = \begin{pmatrix} a_{m,11} & a_{m,12} \\ a_{m,21} & a_{m,22} \end{pmatrix}, \quad \boldsymbol{b}_m = \begin{pmatrix} b_{m,1} \\ b_{m,2} \end{pmatrix}, \tag{32}$$

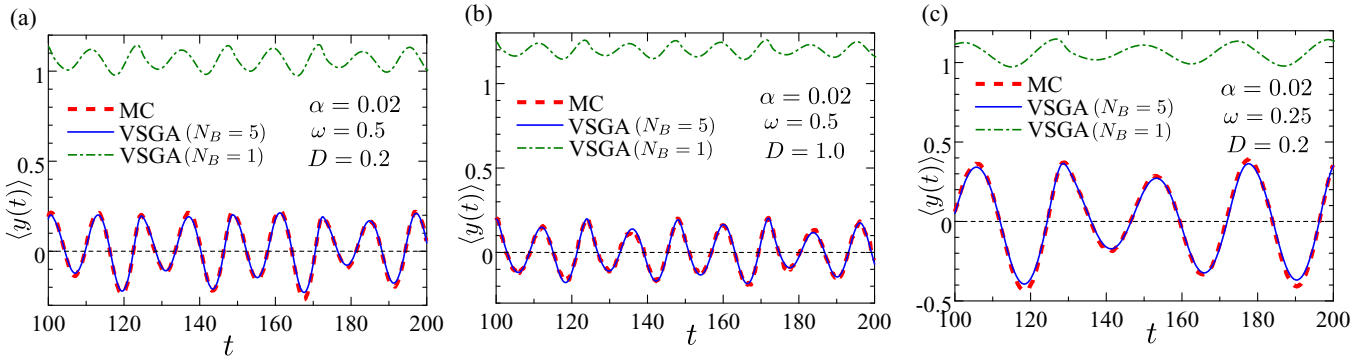

FIG. 7. (Color online) Mean $\langle y(t)\rangle$ as a function of t as obtained by MC simulations (dashed line), the VSGA with $N_B = 5$ (solid line), and the VSGA with $N_B = 1$ (dot-dashed line). The parameters in panels (a)–(c) are the same as in Figs. 5(a)–5(c), respectively.

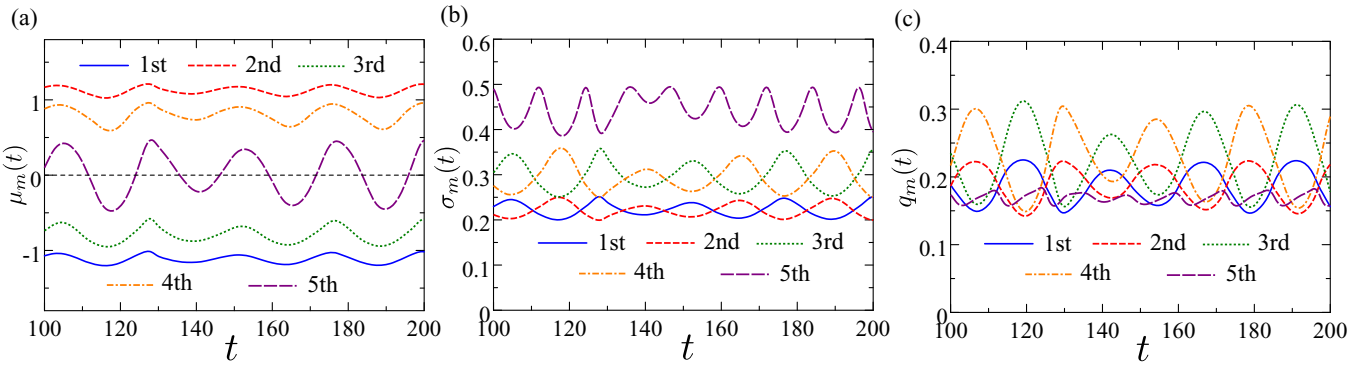

FIG. 8. (Color online) Time evolution of (a) the mean μ_m, (b) the standard deviation σ_m, and (c) the weight q_m, for each Gaussian basis ($N_B = 5$). In panels (a)–(c), the solid, dashed, dotted, dot-dashed, and long-dashed lines represent the quantities for the 1st,2nd, . . . ,5th Gaussian bases, respectively. The parameters are $D = 0.2$, $\alpha = 0.02$, and $\omega = 0.25$.

where $a_{m,12} = a_{m,21}$ ($\boldsymbol{A}_m$ is a symmetric matrix). We require moments of up to the sixth order, i.e., $\int_{-\infty}^{\infty} y^{n_y} z^{n_z} g(y,z;\boldsymbol{A},\boldsymbol{b})dydz$, with $n_y + n_z \leqslant 6$, in order to obtain the DAE. As in the case with white Gaussian noise, Eq. (5) should be satisfied for the normalization, and the resulting $(K+1)$-dimensional DAE is solved numerically.

Figures 10(a) and 10(b) show PDFs $P(y,z;t)$ at $t = 100$, which are calculated by MC simulations and the VSGA with $N_B = 5$, respectively, for $\tau = 0.1$ with $D = 1.0$, $\alpha = 0.02$, and $\omega = 0.5$. To plot the results of the MC simulations as functions of y and z, we employed kernel distributions. Figure 10(c) shows the marginal PDF $P(y;t) = \int_{-\infty}^{\infty} P(y,z;t)dz$, as calculated by MC simulations (circles) and by the VSGA with $N_B = 5$ (dashed curve). Note that these are in good agreement. Figures 10(d) and 10(e) show similar PDFs $P(y,z;t)$, and Fig. 10(f) shows the marginal PDF $P(y;t)$ for $\tau = 0.5$ with $D = 1.0$, $\alpha = 0.02$, and $\omega = 0.5$. As in the one-dimensional case, two bases each are located near the deterministic stable steady states [$(y,z) = (\pm 1,0)$] and one near the deterministic unstable steady state [$(y,z) = (0,0)$]. For $\tau = 0.5$, the peaks of the PDFs are steeper, as can be seen from Figs. 10(d)–10(f). Still the marginal PDF $P(y;t)$ of the VSGA can approximate the MC simulations. These results verify the reliability of the VSGA for the systems with colored Gaussian noise.

Next, we evaluated the dynamical properties of the VSGA by comparing the means $\langle y(t)\rangle$ of the MC simulations and the VSGA. Figure 11 shows the mean $\langle y(t)\rangle$ calculated by the MC simulation (dashed line) and from the VSGA with $N_B = 5$ (solid line), for two different parameters, (a) $\tau = 0.1$ and (b) $\tau = 0.5$; the other parameters were $D = 1.0$, $\alpha = 0.02$, and $\omega = 0.5$ [the parameters settings for Figs. 11(a) and 11(b) correspond to those in Figs. 10(a)–10(c) and 10(d)–10(f), respectively]. In Figs. 11(a) and 11(b), the mean $\langle y(t)\rangle$ obtained from the VSGA is in good agreement with that of the MC simulations, for both τ values. As in the case with white Gaussian noise, the VSGA approximates the two wells with more than two Gaussian distributions, and hence the mean path obtained from the VSGA can accurately approximate the MC simulations. These results show that the VSGA can be applied to a two-dimensional system driven by external forces.

We also computed the correlation C_0 [Eq. (27)] of a chaotically driven system for the case with colored Gaussian noise. Figure 12(a) shows the correlation C_0 as a function of the noise intensity D for $\tau = 0.1$, where other parameters are $\alpha = 0.02$ and $\omega = 0.5$ (C_0 for the VSGA with $N_B = 5$ is shown by a solid line and that for the MC simulations is

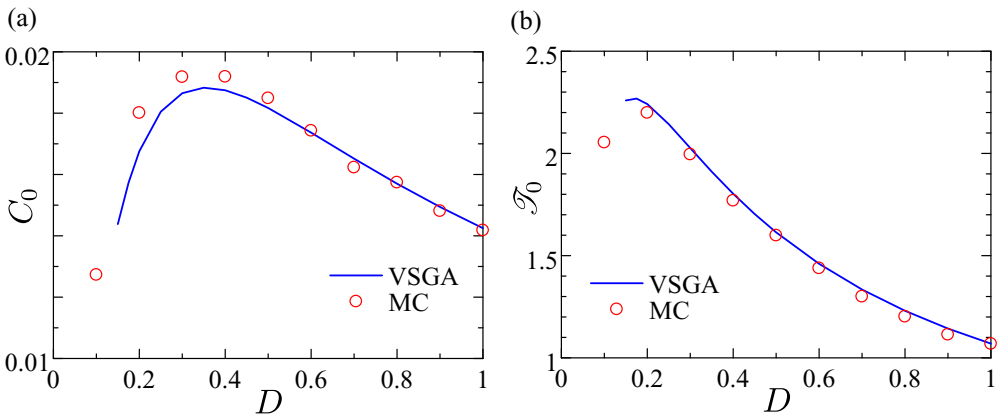

FIG. 9. (Color online) (a) Correlation C_0 [Eq. (27)] and (b) time lag $\mathcal{T}_0$ [Eq. (28)] as a function of the noise intensity D, obtained by the VSGA with $N_B = 5$ (solid line) and by the MC simulations (circles). The parameters are $\alpha = 0.02$ and $\omega = 0.5$. For $D < 0.15$, VSGA could not calculate PDFs.

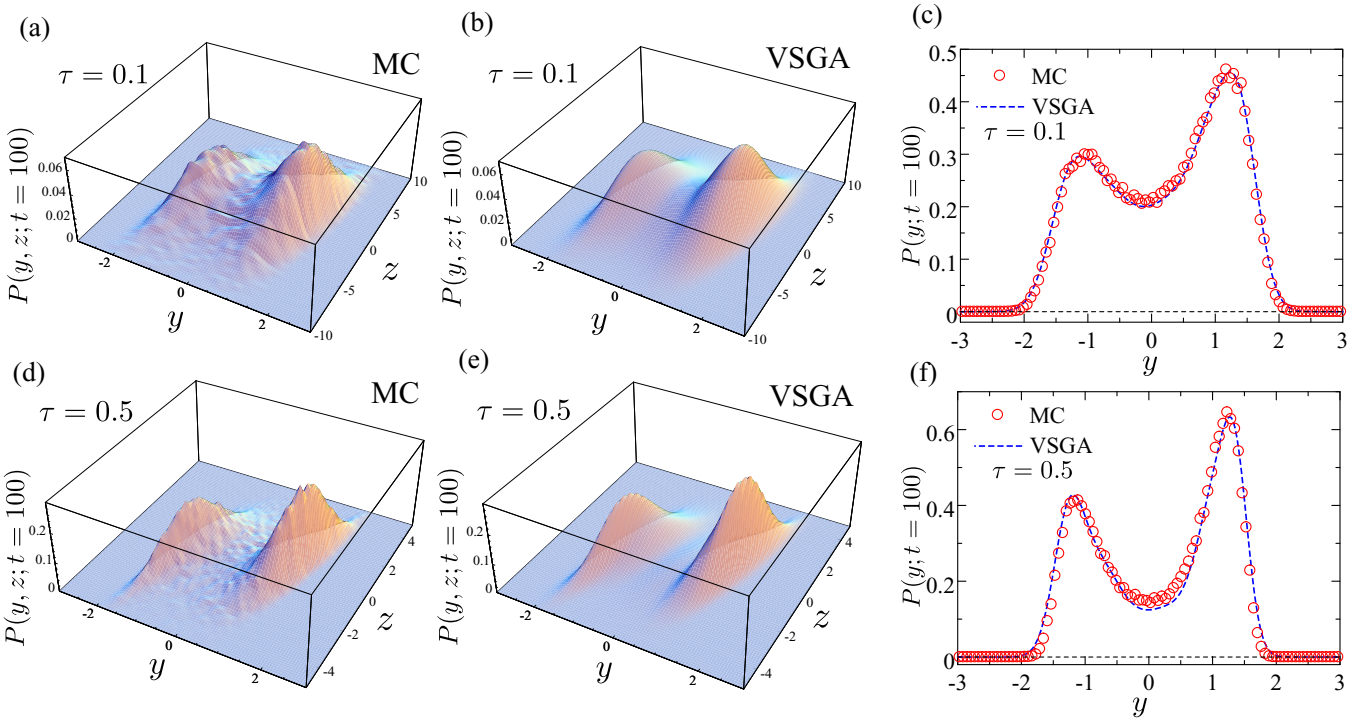

FIG. 10. (Color online) (a),(b),(d),(e) PDFs $P(y,z,;t)$ at time $t = 100$ for two τ settings (a),(b) $\tau = 0.1$ and (d),(e) $\tau = 0.5$ (other parameters are $D = 1.0$, $\alpha = 0.02$, and $\omega = 0.5$), where (a) and (d) are obtained by the MC simulations and (b) and (e) are obtained by the VSGA with $N_B = 5$. (c),(f) Corresponding marginal PDFs $P(y;t)$ for (c) $\tau = 0.1$ and (f) $\tau = 0.5$; results of the VSGA and the MC simulations are shown by dashed lines and circles, respectively.

shown by circles). As seen in Fig. 12(a), C_0 also achieved the maximum value at an intermediate value of D. Comparing the VSGA and MC results shown in Fig. 12(a), we see agreement especially for $D > 0.4$. Figure 12(b) shows the time lag $\mathscr{T}_0$ [Eq. (28)] for the colored-noise case; again $\mathscr{T}_0$ for the VSGA is shown by a solid line and that for MC simulations by circles. From Fig. 12(b), VSGA overevaluated the time lag $\mathscr{T}_0$, implying that the reliability of VSGA in the colored-noise case is worse than the white-noise case. Comparing results of the colored and white-noise cases, we see that the maximum value of C_0 for the colored-noise case is smaller than that for white-noise case which indicates that the colored noise degrades the ASR effect. However, when the noise intensity is not optimal (i.e., $D > 0.6$), the colored noise can better transmit information. We note that the time lag for $\mathscr{T}_0$ with the colored-noise case is larger than that of the white noise.

IV. DISCUSSION AND CONCLUSION

The VSGA introduced in Sec. II can be used to obtain several time-dependent solutions of FPEs. We have shown that our approach can provide very accurate approximations by the superposition of multiple Gaussian distributions for one- and two-dimensional driven systems. We have modeled the mean, variance, and weight as time-dependent parameters. However, as inclusion of the covariance terms [$\boldsymbol{A}_m$ in Eq. (13)] significantly increases the number of parameters, it is one possible approach to approximate the covariance as a constant

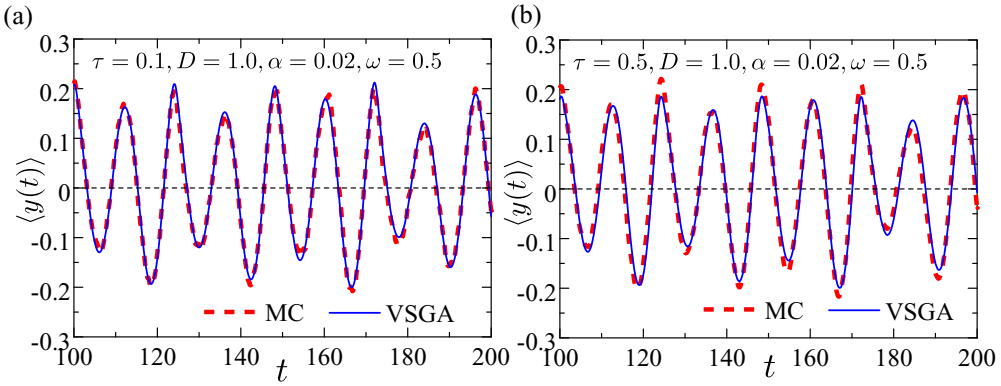

FIG. 11. (Color online) Time dependence of mean $\langle y(t) \rangle$ for (a) $\tau = 0.1$ and (b) $\tau = 0.5$, calculated by MC simulations (dashed curve) and the VSGA with $N_B = 5$ (solid curve). The parameters are $D = 1.0$, $\alpha = 0.02$, and $\omega = 0.5$.

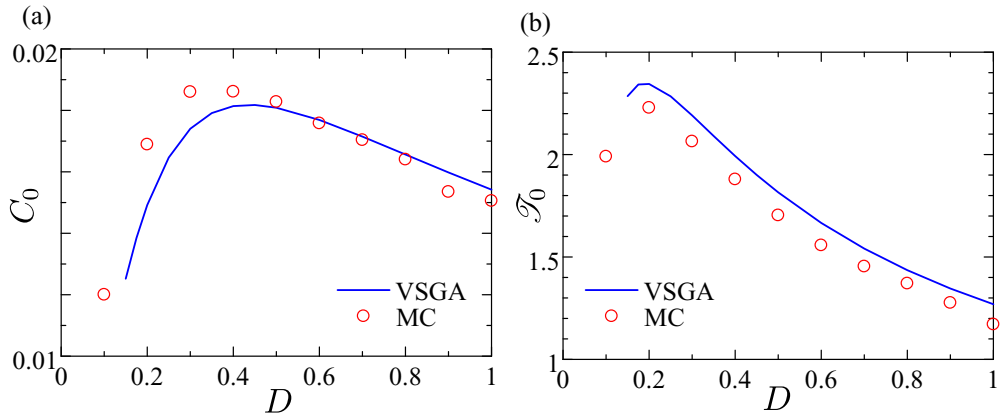

FIG. 12. (Color online) (a) Correlation C_0 [Eq. (27)] and (b) time lag $\mathscr{T}_0$ [Eq. (28)] as a function of the noise intensity D, obtained by the VSGA with $N_B = 5$ (solid line) and by the MC simulations (circles) for the colored-noise case ($\tau = 0.1$). The parameters are $\alpha = 0.02$ and $\omega = 0.5$. For $D < 0.15$, VSGA could not calculate PDFs.

in order to reduce the computational cost. This approach has been considered in the Gaussian wave-packet approximation in quantum mechanics [14] and is referred to as a *frozen* method (the time-dependent covariance model is called a *thawed* method). As shown in Fig. 8, the temporal variation of the standard deviation is around $\sim$0.1, which is smaller than that of the mean. Therefore, if we can first specify the standard deviation of each Gaussian basis, we may ignore the time evolution of the variance. This frozen approximation could dramatically reduce the number of parameters in the VSGA where the parameter size K is

$$K = N_B(N + 1), \tag{33}$$

being linear with respect to the dimension N and its order of N is smaller than that given by Eq. (15).

Although the effectiveness of the VSGA was demonstrated by our numerical results, it has some disadvantages. Because multiple Gaussian distributions are not orthogonal, the VSGA cannot calculate solutions when more than two Gaussian distributions coalesce. In theory, the accuracy of the VSGA increases when more basis functions are used (cf. Fig. 4). However, due to their nonorthogonality, an excessively large number of bases prevents the calculation of the time evolution of the parameters. Also it becomes more difficult to find valid initial values of DAEs for the large N_B cases. Indeed, for the one-dimensional case, the VSGA could not calculate the time evolution with $N_B = 5$ for $D < 0.15$. For such cases, we should reduce N_B in order to enable the calculations. Similarly, for the two-dimensional case, colored noise with a larger time correlation tends to yield steeper peaks, which makes the application of the VSGA difficult with large N_B. Because peaks of PDFs are represented by a few Gaussian bases in VSGA, the required number of bases N_B can be estimated by the number of stable points of the system. When there is no input signal, we can know the number of stable points from a deterministic equation by solving $f_i(\boldsymbol{x}) = 0$ [a time-independent drift in Eq. (1)] and evaluating eigenvalues of the Jacobian matrix around the solutions. If the input signal is weak, it is expected that a driven case has the same number of peaks as the no input case. Still the VSGA can provide a computationally efficient way to calculate the time-dependent dynamics of FPEs. Chaotically driven stochastic systems have often been solved by MC simulations. As shown in Sec. III, the VSGA successfully and very accurately calculated many of the quantities for the system without relying on stochastic approaches.

We applied the VSGA to a quartic bistable potential, where the moments of the Gaussian can be calculated in closed form. The integral in Eq. (12) can be computed analytically if the potentials are represented by polynomials. However, for general nonlinear models, the moment cannot necessarily be represented in closed form. In such situations, we may approximate the drift term $f_i(\boldsymbol{x})$ by the Taylor expansion,

$$f_i(\boldsymbol{x}) \simeq f_i(\boldsymbol{\mu}_g) + \nabla f_i(\boldsymbol{\mu}_g)^\top (\boldsymbol{x} - \boldsymbol{\mu}_g), \tag{34}$$

where $\boldsymbol{\mu}_g$ is the center of the Gaussian distribution in the integrand. When using the linear approximation, obtained results become unreliable when the nonlinearity of a system is strong and/or the variance of basis is large. As for the quartic bistable case, the linear approximation can yield accurate solutions when the noise intensity is sufficiently weak (i.e., the variance of basis is small).

To summarize, we have proposed the VSGA for the time-dependent solution for Langevin equations by using the variational principle for superposition of multiple Gaussian distributions. Because we have shown the effectiveness of the VSGA in strongly nonlinear systems, the VSGA is expected to be used for many real-world problems. Applications of the VSGA to other problems, such as to stochastic models of gene expression [2,3], are left to our future study.

ACKNOWLEDGMENTS

This work was supported by KAKENHI Grant No. 25870171 from the Japan Society for the Promotion of Science.

APPENDIX A: RELATION TO CONVENTIONAL MULTIVARIATE GAUSSIAN REPRESENTATION

The N-dimensional multivariate Gaussian distribution is generally given by the representation

$$\mathcal{N}(\boldsymbol{x};\boldsymbol{\mu},\boldsymbol{\Sigma}) = \frac{1}{(2\pi)^{N/2}\sqrt{|\boldsymbol{\Sigma}|}} \exp\left\{ -\frac{1}{2}(\boldsymbol{x}-\boldsymbol{\mu})^{\top}\boldsymbol{\Sigma}^{-1}(\boldsymbol{x}-\boldsymbol{\mu})\right\}, \tag{A1}$$

where $\boldsymbol{\mu}$ is the mean vector (column vector) and $\boldsymbol{\Sigma}$ is the covariance matrix (positive definite). In Eq. (A1), $|\boldsymbol{\Sigma}|$ denotes the determinant of $\boldsymbol{\Sigma}$. The mixture of multivariate Gaussian distributions is given by

$$P(\boldsymbol{x};\{\boldsymbol{\mu}_m\},\{\boldsymbol{\Sigma}_m\},\{q_m\}) = \sum_{m=1}^{N_B} q_m \mathcal{N}(\boldsymbol{x};\boldsymbol{\mu}_m,\boldsymbol{\Sigma}_m), \tag{A2}$$

where q_m is the weight ($\sum_{m=1}^{N_B} q_m = 1$). This conventional representation and Eq. (13) are related in the following way:

$$\boldsymbol{A}_m = \frac{\boldsymbol{\Sigma}_m^{-1}}{2}, \tag{A3}$$

$$\boldsymbol{b}_m = \boldsymbol{\Sigma}_m^{-1}\boldsymbol{\mu}_m, \tag{A4}$$

$$r_m = \frac{q_m}{(2\pi)^{N/2}\sqrt{|\boldsymbol{\Sigma}_m|}} \exp\left\{ -\frac{1}{2}\boldsymbol{\mu}_m^{\top}\boldsymbol{\Sigma}_m^{-1}\boldsymbol{\mu}_m\right\}. \tag{A5}$$

According to Eq. (A3), $\boldsymbol{A}_m$ is positive definite since it is the inverse of a positive definite matrix (Σ is positive definite). The inverse transform of Eqs. (A3)–(A5) is

$$\boldsymbol{\Sigma}_m = \frac{1}{2}\boldsymbol{A}_m^{-1}, \tag{A6}$$

$$\boldsymbol{\mu}_m = \frac{1}{2}\boldsymbol{A}_m^{-1}\boldsymbol{b}_m, \tag{A7}$$

$$q_m = \frac{r_m \pi^{N/2}}{\sqrt{|\boldsymbol{A}_m|}} \exp\left\{ \frac{1}{4}\boldsymbol{b}_m^{\top}\boldsymbol{A}_m^{-1}\boldsymbol{b}_m\right\}. \tag{A8}$$

In Eqs. (A3)–(A8), we used the fact that $\boldsymbol{A}_m$ is symmetric.

APPENDIX B: INITIAL VALUES OF DAE

One of the difficulties in our approach is to find valid initial values for the DAEs. Unlike conventional (explicit) ordinary differential equations, DAEs must satisfy an equality condition, and some parameters should be determined numerically by that equality (in our implementation, this was done automatically by *Mathematica 10*). We found that calculating the equality is difficult in some cases. For larger noise intensities D (for both the white- and colored-noise cases) and for smaller correlation times τ (for the colored-noise case), it is relatively easy to find valid initial values for the DAE. Therefore, when finding initial values when D is smaller, we first find valid initial values with $D = 1.0$ (large D value) and then iterate the calculations, adopting the converged stationary values of the preceding D values as the initial values used to find the next D value. It is also possible to adjust the system by making D (or τ) a time-dependent parameter and assuming that D (τ) decreases (increases) over time starting from large D (small τ) value. This time-dependent technique was employed for the $\tau = 0.5$ case.

[1] V. Kampen, *Stochastic Process Theory in Physics and Chemistry* (North-Holland, Amsterdam, 1992).
[2] Y. Hasegawa and M. Arita, J. R. Soc., Interface **11**, 20131018 (2014).
[3] Y. Hasegawa and M. Arita, Phys. Rev. Lett. **113**, 108101 (2014).
[4] F. Ritort, in *Advances in Chemical Physics*, edited by S. A. Rice, (John Wiley & Sons, Hoboken, 2007), Vol. 137, pp. 31–123.
[5] U. Seifert, Rep. Prog. Phys. **75**, 126001 (2012).
[6] H. Huang and N. M. Ghoniem, Phys. Rev. E **51**, 5251 (1995).
[7] R. Rodriguez and H. C. Tuckwell, Phys. Rev. E **54**, 5585 (1996).
[8] H. C. Tuckwell and J. Jost, Phys. A (Amsterdam, Neth.) **388**, 4115 (2009).
[9] E. J. Heller, J. Chem. Phys. **64**, 63 (1976).
[10] A. D. McLachlan, Mol. Phys. **8**, 39 (1964).
[11] P. A. M. Dirac, Math. Proc. Camb. Philos. Soc. **26**, 376 (1930).
[12] J. Frenkel, *Wave Mechanics, Advanced General Theory* (Clarendon Press, Oxford, 1934).
[13] J. Broeckhove, L. Lathouwers, E. Kesteloot, and P. Van Leuven, Chem. Phys. Lett. **149**, 547 (1988).
[14] R. T. Skodje and D. G. Truhlar, J. Chem. Phys. **80**, 3123 (1984).
[15] G. A. Worth, M. A. Robb, and I. Burghardt, Faraday Discuss. **127**, 307 (2004).
[16] J. O. Zoppe, M. L. Parkinson, and M. Messina, Chem. Phys. Lett. **407**, 308 (2005).
[17] G.-K. Er, Int. J. Nonlinear Mech. **33**, 201 (1998).
[18] H. J. Pradlwarter, Int. J. Nonlinear Mech. **36**, 1135 (2001).
[19] G. Terejanu, P. Singla, T. Singh, and P. D. Scott, J. Guid. Control Dyn. **31**, 1623 (2008).
[20] M. Di Paola and A. Sofi, Probab. Eng. Mech. **17**, 369 (2002).
[21] H. Risken, *The Fokker-Planck Equation: Methods of Solution and Applications*, 2nd ed. (Springer, Berlin, 1989).
[22] G. W. Harrison, Numer. Methods Partial Differ. Equations **4**, 219 (1988).
[23] P. Kumar and S. Narayanan, Sadhana **31**, 445 (2006).
[24] J. C. Whitney, J. Comput. Phys. **6**, 483 (1970).
[25] T. Wilhelm, BMC Syst. Biol. **3**, 90 (2009).
[26] P. Jung, Phys. Rep. **234**, 175 (1993).
[27] J. J. Collins, C. C. Chow, and T. T. Imhoff, Phys. Rev. E **52**, R3321 (1995).
[28] J. J. Collins, C. C. Chow, A. C. Capela, and T. T. Imhoff, Phys. Rev. E **54**, 5575 (1996).
[29] R. Benzi, A. Sutera, and A. Vulpiani, J. Phys. A **14**, L453 (1981).
[30] B. McNamara and K. Wiesenfeld, Phys. Rev. A **39**, 4854 (1989).

[31] L. Gammaitoni, P. Hänggi, P. Jung, and F. Marchesoni, Rev. Mod. Phys. **70**, 223 (1998).

[32] M. D. McDonnell, N. G. Stocks, C. E. M. Pearce, and D. Abbott, *Stochastic Resonance* (Cambridge University Press, Cambridge, UK, 2008).

[33] M. D. McDonnell and D. Abbott, PLoS Comput. Biol. **5**, e1000348 (2009).

[34] U. M. Ascher and L. R. Petzold, *Computer Methods for Ordinary Differential Equations and Differential-algebraic Equations* (SIAM, Philadelphia, 1998).

[35] O. E. Rössler, Phys. Lett. A **57**, 397 (1976).

[36] A. Silchenko, T. Kapitaniak, and V. Anishchenko, Phys. Rev. E **59**, 1593 (1999).